Antireflective properties of porous Si nanocolumnar structures with graded refractive index layers

Sung Jun Jang,[1] Young Min Song,[1] Jae Su Yu,[2] Chan Il Yeo,[1] and Yong Tak Lee[1,3,4,*]

[1]*School of Information and Communications, Gwangju Institute of Science and Technology, 1 Oryong-dong, Buk-gu, Gwangju 500-712, South Korea*

[2]*Department of Electronics and Radio Engineering, Kyung Hee University, 1 Seocheon-dong, Giheung-gu, Yongin-si, Gyeonggi-do 446-701, South Korea*

[3]*Graduate Program of Photonics and Applied Physics, Gwangju Institute of Science and Technology, 1 Oryong-dong, Buk-gu, Gwangju 500-712, South Korea*

[4]*Department of Nanobio Materials and Electronics, Gwangju Institute of Science and Technology, 1 Oryong-dong, Buk-gu, Gwangju 500-712, South Korea*

**Corresponding author: ytlee@gist.ac.kr*

Received May 19, 2010; revised October 11, 2010; accepted November 27, 2010; posted December 9, 2010 (Doc. ID 128723); published January 13, 2011

We report on the antireflective characteristics of porous silicon (Si) nanocolumnar structures consisting of graded refractive index layers and carry out a rigorous coupled-wave analysis simulation. The refractive index of Si is gradually modified by a tilted angle electron beam evaporation method. For the fabricated Si nanostructure with a Gaussian index profile of 100 nm, reflectivity (R) of less than 7.5% is obtained with an average value of approximately 2.9% at the wavelength region of 400–800 nm. The experimental results are reasonably consistent with the simulated results for the design of antireflective Si nanostructures.

OCIS codes: 050.6624, 040.5350, 260.2710.

Antireflection coatings (ARCs) have been widely used to effectively reduce surface reflection in various optical and optoelectronic devices. In particular, solar cells require a broadband and omnidirectional ARC to improve the cell efficiency. There have been many efforts to fabricate broadband ARC structures, using a variety of techniques. Subwavelength grating structures, e.g., moth eyes, and truncated and tapered cone structures, which have a smaller period than the light wavelength, have been demonstrated [1–3]. However, nanoscale structures require expensive nanolithography and dry etching.

Optical thin films with a graded refractive index can also reduce Fresnel reflection at the surface [4–6]. The shadowing effect in oblique angle electron beam (e-beam) deposition leads to a gradual change in the refractive index via the introduction of air voids within the films [7]. Recently, in efforts to form graded refractive index ARCs, SiO_2, TiO_2, and MgF_2 films with low refractive indices (low-n) were grown by oblique angle deposition [8,9]. However, the dielectric films have low thermal conductivities and, hence, poor heat dissipation capability. On the other hand, evaporated amorphous silicon (Si) films have relatively better thermal conductivity, and their refractive index can be changed over a wide range because Si has a high refractive index. In this Letter, we describe the fabrication of Si nanostructures with different graded refractive index profiles designed using a rigorous coupled-wave analysis (RCWA) by tilted angle e-beam evaporation for ARCs. The incident angle dependent antireflection properties of porous Si graded refractive index structures with nanocolumns were studied for Si solar cell applications.

Low-n Si films were deposited on a (100) Si substrate by tilted angle evaporation using multiangled sample holders at angles ranging from 0° to 88°. To design a graded refractive index ARC structure, the optical property was experimentally investigated for low-n Si films at various incident angles of e-beam flux by spectroscopic ellipsometry measurement. Figure 1 shows the extinction coefficient as a function of wavelength for porous Si nanocolumnar films deposited at $\theta_{\text{tilt}} = 0°$, 40°, 55°, 70°, and 88°. The inset shows the corresponding refractive index spectra. The extinction coefficient was reduced rapidly to below 0.22 at 400–800 nm until $\theta_{\text{tilt}} = 55°$ and thereafter fell slowly. The refractive index was decreased from 3.33 at $\theta_{\text{tilt}} = 0°$ to 1.09 at $\theta_{\text{tilt}} = 88°$ in a wavelength range of 400–800 nm as the incident angle of the e-beam flux was increased. Moreover, the nanocolumns become more separated by substantial voids. For tilted angle deposition, the subsequently arriving Si particles cannot reach the self-shadowing region

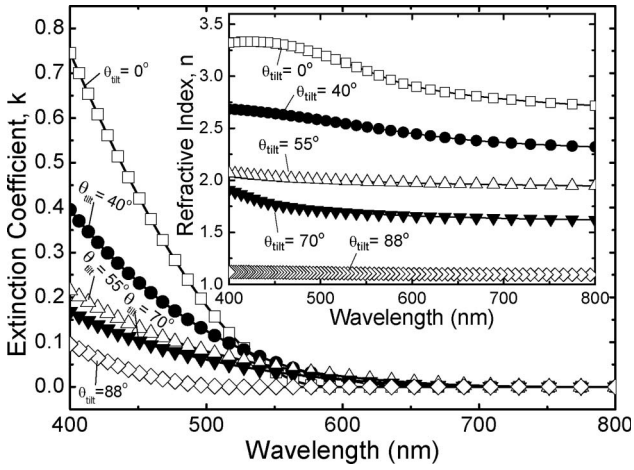

Fig. 1. Extinction coefficient as a function of wavelength for low-n Si films deposited at $\theta_{\text{tilt}} = 0°$, 40°, 55°, 70°, and 88°. The inset shows the corresponding refractive index spectra.

0146-9592/11/020253-03$15.00/0

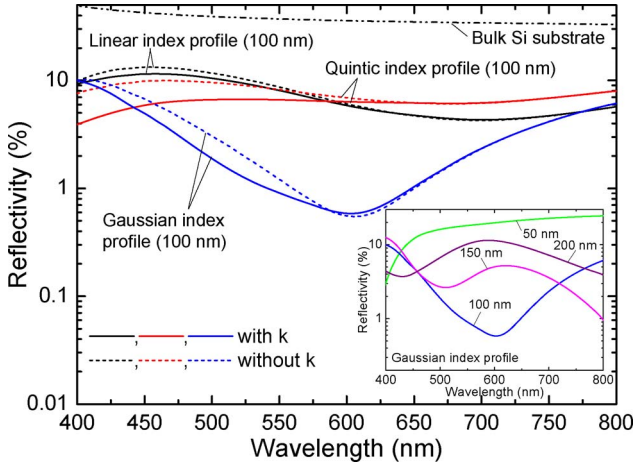

Fig. 2. (Color online) Calculated reflectivity as a function of wavelength at normal incidence for 100-nm-thick Si films for linear, quintic, and Gaussian index profiles, respectively. For comparison, the dashed curves show the calculated reflectivities without considering the extinction coefficient. The inset shows the calculated reflectivity spectra for Gaussian index profiles of 50, 100, 150, and 200 nm.

caused by the columns developed from initial nuclei on the substrate.

Figure 2 shows the calculated reflectivity as a function of the wavelength at normal incidence for 100-nm-thick Si films with linear, quintic, and Gaussian index profiles. The inset shows the calculated reflectivity spectra for Gaussian index profiles of 50, 100, 150, and 200 nm. For linear, quintic, and Gaussian index profiles, the refractive indices between air and Si substrate are given by $n(x) = n_{\text{air}} + (n_{\text{si}} - n_{\text{air}})x$, $n(x) = n_{\text{air}} + (n_{\text{Si}} - n_{\text{air}})(10x^3 - 15x^4 + 6x^5)$, and $n(x) = n_{\text{air}} + (n_{\text{Si}} - n_{\text{air}}) \exp[-(x-1)^2/0.4^2]$, respectively [10]. Here, x is the film thickness, n_{air} is the refractive index of air, and n_{Si} is the refractive index of Si. To approximately fit these profiles, porous Si nanocolumnar films, which are composed of four different layers deposited at each tilted angle, were employed in this experiment as ARCs. The thicknesses of the four layers at different tilted angles and the measured refractive indices for different graded index profiles are shown in Table 1. To evaluate the design of ARCs using different tilted angle evaporated Si films, an RCWA simulation was carried out to estimate the reflectivity. The designed films with graded refractive index profiles exhibited relatively low reflectivities of $R < 10\%$ in the visible wavelength range compared to the bulk Si substrate (i.e., $R > 32\%$). For linear and quintic index profiles, the average reflectivities were 7.77% and 5.85%, respectively, at 400–800 nm. For the Gaussian index profile, the lowest average reflectivity of 400–800 nm was 3.05%. For comparison, the dashed curves show the calculated reflectivities without considering the extinction coefficient. The difference between reflectivities calculated with and without considering the extinction coefficient is very small, although there exists a distinct discrepancy in the reflectivity in the short wavelength region for the quintic index profile. The reflectivity depends strongly on the thickness of the Si films and is minimized at 100 nm for the Gaussian index profile as shown in the inset of Fig. 2.

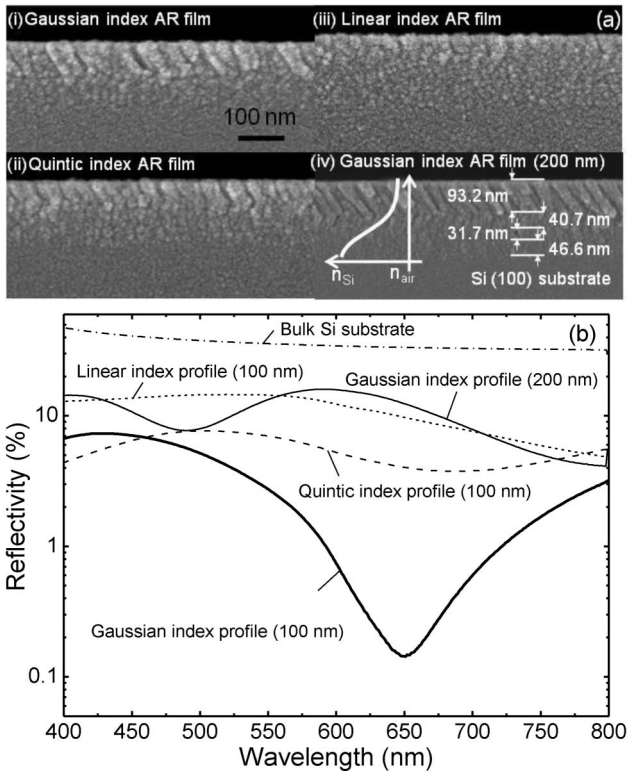

Fig. 3. (a) Cross-sectional SEM images of porous Si nanocolumnar films deposited on Si substrate for (i) Gaussian index profile (100 nm), (ii) quintic index profile (100 nm), (iii) linear index profile (100 nm), and (iv) Gaussian index profile (200 nm); (b) measured reflectivity spectra at normal incidence with different index profiles.

Figure 3(a) shows the cross-sectional scanning electron microscope (SEM) images of porous Si nanocolumnar films deposited on a Si substrate for (i) a Gaussian index profile (100 nm), (ii) a quintic index profile (100 nm), (iii) a linear index profile (100 nm), and (iv) a Gaussian index profile (200 nm). Although it is rather difficult to discriminate the boundaries between the four structural layers for 100 nm graded index layers, they become more distinct for the thicker graded index layer. For a Gaussian index profile of 200 nm, the four-layer structure was distinctly observed with its thicknesses from the SEM measurement as can be seen in part (iv) of Fig. 3(a). The measured individual thicknesses are

Table 1. Thicknesses of Four Layers at Different Tilted Angles and Their Measured Refractive Indices for Different Graded Index Profiles

Layer Number	θ_{tilt}	n (at 633 nm)	t_{linear} (100 nm)	t_{quintic} (100 nm)	t_{Gaussian} (100 nm)	t_{Gaussian} (200 nm)
1	70°	1.65	15 nm	29 nm	44.8 nm	89.6 nm
2	55°	1.96	27.6 nm	17.2 nm	18.2 nm	36.4 nm
3	40°	2.41	30.8 nm	17 nm	14.8 nm	29.6 nm
4	0°	2.85	26.8 nm	37 nm	22.4 nm	44.8 nm

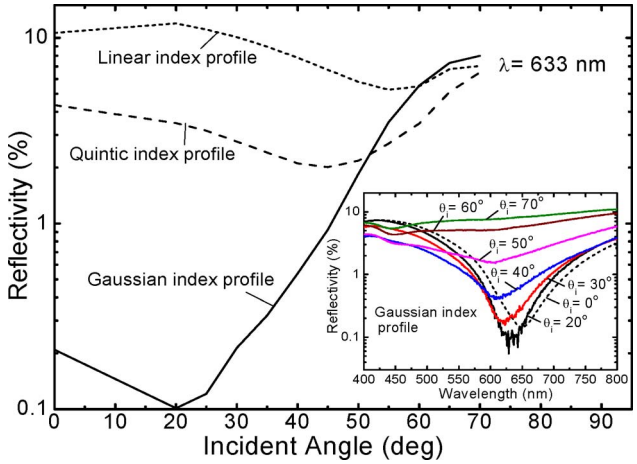

Fig. 4. (Color online) Light incident angle dependent reflectivity of 100-nm-thick antireflective (AR) films at a wavelength of 633 nm for linear, quintic, and Gaussian index profiles. The inset shows the measured reflectivity spectra of the AR film with a Gaussian index profile of 100 nm for different angles of incident light.

roughly similar to the theoretical thickness values. The measured reflectivity spectra at normal incidence for the porous Si nanocolumnar films with different index profiles are shown in Fig. 3(b). The reflectivity was measured using a spectrophotometer over a wavelength range from 400 nm to 800 nm. Overall, the measurement and theoretical results are in reasonable agreement, although there is a slight redshift in the experimental data due to deviations in the refractive index and thickness in the fabrication of the Si nanostructures. As anticipated from the theoretical simulations, the Gaussian index profile of 100 nm exhibits the lowest reflectivity in the visible wavelength range. The measured average reflectivities were 10.89% and 5.45% at wavelengths of 400–800 nm for linear and quintic index profiles of 100 nm, respectively. For a 100-nm-thick Si nanostructure with a Gaussian index profile, reflectivity of less than 7.5% was measured over a wavelength range of 400–800 nm, leading to an average reflectivity of ~2.9%. As shown in the inset of Fig. 2, for Gaussian index profiles below or above 100 nm, the reflectivity was found to be theoretically reduced. It is clear that the Gaussian index profile of 200 nm has much higher reflectivity values compared to the Gaussian index profile of 100 nm.

Figure 4 shows the light incident angle dependent reflectivity of 100-nm-thick porous Si nanocolumnar films at a wavelength of 633 nm for linear, quintic, and Gaussian index profiles. The inset shows the measured reflectivity spectra of the porous Si nanocolumnar film with a Gaussian index profile of 100 nm for different angles of incident light. At light incident angles ranging from $\theta_i = 0°$ to $\theta_i = 70°$, relatively low reflectivity at 633 nm was obtained for the Gaussian index profile of 100 nm compared to the other profiles. The Si nanostructure with a Gaussian index profile of 100 nm results in wide-angle antireflective characteristics of $R < 10\%$ at incident angles of $\theta_i = 0$–$70°$ at wavelengths of 400–800 nm. In the light incident angle region of $\theta_i = 0$–$50°$, which is particularly important for practical solar cell applications, the reflectivity was less than 5% in the wavelength range of 400–800 nm.

In summary, we fabricated Si nanocolumnar structures with linear, quintic, and Gaussian index profiles using four layers deposited at different tilted angles by an e-beam evaporator. To suppress surface reflection, Si-nanostructure-based ARCs were designed by fitting the thicknesses of the four layers with their measured refractive index to the graded index profiles using an RCWA simulation. For a Gaussian index profile of 100 nm, a wide spectrum and angle antireflective properties less than 10% at $\theta_i = 0$–$70°$ (particularly, $R < 5\%$ at $\theta_i = 0$–$45°$) were observed in a wavelength range of 400–800 nm, indicating reasonable agreement with the theoretical results. From these results, the Si nanocolumnar structure with an optimally graded index profile is expected to be a candidate broadband omnidirectional ARC for solar cell applications.

This work was supported by the IT R&D program of the Ministry of Knowledge Economy (MKE) (2007-F-045-03), by the World Class University (WCU) program of the Ministry of Education, Science, and Technology (MEST) (Project No. R31-2008-000-10026-0), and by the Core Technology Development Program for Next-Generation Solar Cells of the Research Institute for Solar and Sustainable Energies (RISE), Gwangju Institute of Science and Technology (GIST).

References

1. A. Szeghalmi, M. Helgert, R. Brunner, F. Heyroth, U. Gosele, and M. Knez, Appl. Opt. **48**, 1727 (2009).
2. Y. F. Huang, S. Chattopadhyay, Y. Jen, C. Peng, T. Liu, Y. Hsu, C. Pan, H. Lo, C. Hsu, Y. Chang, C. Lee, K. Chen, and L. Chen, Nat. Nanotechnol. **2**, 770 (2007).
3. Y. M. Song, J. S. Yu, and Y. T. Lee, Opt. Lett. **35**, 276 (2010).
4. A. Mahdjoub and L. Zighed, Thin Solid Films **478**, 299 (2005).
5. S. Lange, H. Bartzsch, P. Frach, and K. Goedicke, Thin Solid Films **502**, 29 (2006).
6. M. Lipinski, A. Kaminski, J. F. Lelievre, M. Lemiti, E. Fourmond, and P. Zieba, Phys. Status Solidi C **4**, 1566 (2007).
7. J. Q. Xi, M. F. Schubert, J. K. Kim, E. F. Schubert, M. Chen, S. Y. Lin, W. Liu, and J. A. Smart, Nat. Photon. **1**, 176 (2007).
8. S. Chhajed, M. F. Schubert, J. K. Kim, and E. F. Schubert, Appl. Phys. Lett. **93**, 251108 (2008).
9. C. C. Jaing, M. C. Liu, C. C. Lee, W. H. Cho, W. T. Shen, C. J. Tang, and B. H. Liao, Appl. Opt. **47**, C266 (2008).
10. M. Chen, H. C. Chang, A. S. P. Chang, S. Y. Lin, J. Q. Xi, and E. F. Schubert, Appl. Opt. **46**, 6533 (2007).